Acta Materialia 250 (2023) 118878

Contents lists available at ScienceDirect

Acta Materialia

journal homepage: www.elsevier.com/locate/actamat

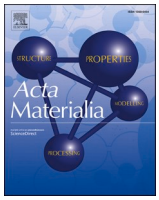

Full length article

Small-scale fracture mechanical investigations on grain boundary doped ultrafine-grained tungsten

Michael Wurmshuber [a,*], Markus Alfreider [a], Stefan Wurster [b], Michael Burtscher [a], Reinhard Pippan [b], Daniel Kiener [a]

[a] Department Materials Science, Montanuniversität Leoben, Jahnstraße 12, Leoben 8700, Austria
[b] Erich Schmid Institute of Materials Science, Austrian Academy of Sciences, Jahnstraße 12, Leoben 8700, Austria

The inherent brittleness of the refractory metal tungsten represents a major challenge for its application as divertor material in future nuclear fusion reactors. Grain refinement to the ultrafine-grained regime is a promising strategy to increase the fracture toughness of W, but it also promotes intercrystalline crack growth. Therefore, the strengthening of grain boundary cohesion in W is of great importance. In this work, grain boundary doping with B and Hf, two elements that were identified in previous work to increase bending strength and ductility, is applied to ultrafine-grained W. The fracture toughness is measured utilizing small-scale testing techniques. Fracture mechanical experiments on the microscale provide a plethora of challenges to correctly assess size-independent toughness values, which are presented and discussed within this work. It was found that the toughness of W can be under- and overestimated, depending on the sample dimensions and plastic zone size. When assessing the valid and size-independent fracture toughness measured for the differently doped W specimen, doping with the strengthening element B maintained the already remarkably high toughness of the undoped ultrafine-grained W of around 20 MPa$\sqrt{m}$. The samples doped with Hf even improved the fracture toughness to values of up to 27 MPa$\sqrt{m}$. Hence, the effects of GB doping on the fracture toughness of ultrafine-grained W are explored, while simultaneously the influence of sample dimensions on measured fracture toughness is discussed. These insights are expected to have a great impact on the development of superior materials for use in harsh environments, as well as the application of small-scale fracture mechanical experiments, as used, for example, in the assessment of control samples in nuclear technology.

1. Introduction

Exhibiting the highest melting point of any pure chemical element (3422 °C), high intrinsic strength and many more favorable properties [1], tungsten is frequently considered for high-performance applications in the harshest environments, for example as structural material in the divertor part of nuclear fusion reactors [2–7]. However, the limited ductility and inherent brittleness of the refractory metal oftentimes represent critical obstacles for a successful and safe employment of W in such applications. In recent years, many strategies to improve ductility and fracture toughness of W have been investigated [3,4,7–9] and a reduction in grain size by either cold-rolling [10–13], wire-drawing [14–17] or severe plastic deformation (SPD) [18,19] showed promising results in elevating the overall mechanical properties. As the smaller grain size and, consequently, larger amount of grain boundaries within W favor a preferential intercrystalline fracture mode [20–23], strengthening the grain boundary (GB) cohesion has potential to further enhance the mechanical properties and especially toughness of W. By applying the concept of grain boundary segregation engineering (GBSE) [24–32] and by selecting ab-initio informed doping elements [33,34], it was shown that doping of ultrafine-grained (ufg) W with B and Hf can significantly improve the bending strength and bending ductility [35], respectively.

In this work, the effect of these doping elements on the fracture toughness of ufg W, fabricated by high-pressure torsion (HPT), is investigated. As the sample volume of such SPD-processed materials is limited and a microstructural gradient is present, small-scale fracture mechanical experiments have to be utilized. By far the most popular test configuration on the microscale is the notched cantilever bending test [36–45] (see Fig. 1). For semi-brittle materials, such as ufg W, the application of such experiments is rather challenging, as the decent ductility and extremely small sample dimensions lead to validity issues [38,40,46]. Thus, in this work fracture mechanical experiments are performed for different cantilever dimensions of the various undoped and doped materials. The validity of the experiments and the micromechanical mechanisms behind perceived invalid toughness values are discussed. These insights are not only valuable for the concrete case at hand, but for micromechanical fracture experiments as a whole. Small-scale fracture mechanical tests can also play an important role in the application of W in fusion reactors: In order to evaluate the risk of

* Corresponding author.
E-mail address: michael.wurmshuber@unileoben.ac.at (M. Wurmshuber).

https://doi.org/10.1016/j.actamat.2023.118878
Received 5 August 2022; Received in revised form 25 February 2023; Accepted 23 March 2023
Available online 24 March 2023

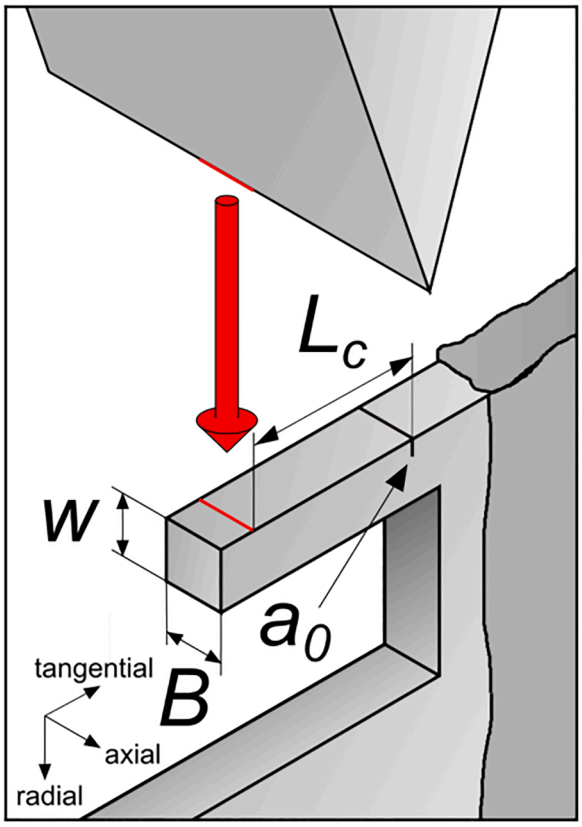

Fig. 1. Micromechanical testing setup for notched cantilever bending fracture experiments.

continued operation, it is common practice in nuclear fission energy to place control samples made out of the structural reactor-material inside the reactor. This way, the control sample experiences the same environmental conditions, such as irradiation and corrosion, as the employed reactor material. Therefore, in order to assess the mechanical property changes over time due to these environmental effects without stopping the fission operation and disassembling the reactor, one can simply test this control sample. These mechanical tests have in recent years increasingly been performed in smaller and smaller dimensions, in order not to "waste" any control sample material for the years to come [47–49]. It is reasonable to assume that a similar approach can be employed in novel nuclear fusion reactors. Additionally, irradiation studies on potential reactor materials are frequently performed using ion-irradiation, instead of time-consuming neutron irradiation. Here, the evaluation of mechanical properties using small-scale testing techniques is inevitable, given the shallow penetration depth of ions and therefore limited volume of irradiated material [44,47–56]. Hence, the correct evaluation of fracture toughness on the microscale for a material such as ufg W is crucial.

Therefore, this work investigates the effect of GB doping on the fracture toughness of ufg W, while in addition important remarks on the sensitive topic of sample dimensions for valid small-scale fracture experiments are made.

2. Material and methodology

2.1. Material

The materials investigated in this work are ufg W samples as produced in [35]. The undoped, boron-doped and hafnium-doped samples from this work are all fabricated from powders using a combination of cold-compacting, annealing and subsequent HPT deformation at 400 °C under a nominal pressure of 12 GPa for about 1 rotation [35,57]. The amount of B and Hf doping elements was adjusted to between 3 and 5 at. %. A boron-doped sample underwent an additional low-temperature annealing at 500 °C for 5 h after the HPT processing, which resulted in a hardening-by-annealing effect and a more pronounced GB segregation of B. This sample is hereinafter marked "W-B ann.". The result from this fabrication process are specimen disks with a diameter of 6 mm and a thickness of ~0.6 mm. These material disks show a microstructural gradient from the disk center to the edge, with the desired microstructure and a grain size of 140–160 nm only being present at the outer regions of the sample disks at a radius of 3 mm.

An overview of the described microstructural features and GB chemistry of the respective materials is depicted in Fig. 2. SEM micrographs and measured grain sizes of the ufg W variants are shown in Fig. 2a–d. Fig. 2e displays results from APT measurements of B content at GBs. It is apparent that annealing of the B-doped material leads to a pronounced segregation of B at and around the GB compared to the unannealed W-B material. Fig. 2f shows an EDX map of large HfO_2 particles present in the Hf-doped ufg W sample, suggesting that Hf attracts and binds O and therefore indirectly strengthens GBs in W. Fig. 2g displays the microstructure of the annealed B-doped material captured by STEM.

2.2. Small-scale fracture mechanical tests

Due to the aforementioned microstructural gradient within the sample disks and limited sample volume containing the studied microstructure, the fracture toughness of the materials was investigated by small-scale fracture mechanical experiments. For this purpose, cantilevers were fabricated at the desired location, i.e. at a radius of 3 mm from the disk center, using a dual-beam FIB-SEM (LEO 1540 XB and Zeiss Auriga, both Zeiss GmbH, Germany) and a small pre-notch was introduced to the cantilevers using a FIB milling current of 30 pA (see Fig. 1). Cantilevers with approximate dimensions of 3 × 3 × 10 μm as well as 8 × 8 × 30 μm were fabricated for all investigated materials. Additionally, a combined femtosecond laser (Origami 10 XP, Onefive GmbH, Switzerland) [58] and FIB approach was utilized to prepare larger cantilevers (approximate dimensions of 30 × 30 × 110 μm) in both the undoped W and the hafnium-doped sample. The ratio of initial crack length and sample width $\frac{a_0}{w}$ was kept constant at approximately 0.1 for all investigated sample dimensions. Examples for (already tested) cantilevers with different sample dimensions and their fracture surfaces are shown in Fig. 3. All cantilevers were fabricated with the crack growth direction towards the sample disk center (radial direction). As even the largest cantilever dimensions are still rather small for a semi-brittle material such as ufg W, the small scale yielding criterion [40,46,59,60] (Eq. (1)) is not met for any specimen and linear elastic fracture mechanics is not applicable to the cantilever experiments:

$$B,\ (w - a_0)\ >\ 2.5\left(\frac{K_Q}{\sigma_y}\right)^2 \tag{1}$$

With B being the sample thickness, w the sample width and a_0 the initial crack length of the FIB-milled notch (compare with Fig. 1). K_Q represents the conditional critical stress intensity factor of the material measured in the experiment and σ_y the yield strength of the material. Note that it is common practice in fracture mechanics to denote the sample width with a capital W. However, to avoid confusion with the chemical symbol for the element tungsten, a lower case w was chosen as symbol for the sample width in this work. According to Eq. (1), the thickness and ligament length of each specimen has to be at least 110 μm in order to fulfill the criterion and to be able to apply linear elastic fracture mechanics (LEFM) on undoped ufg W.

As no sample fulfills Eq. (1), elastic-plastic fracture mechanics (EPFM) has to be applied instead in order to derive valid fracture toughness values [46]. As a measure of fracture toughness within EPFM,

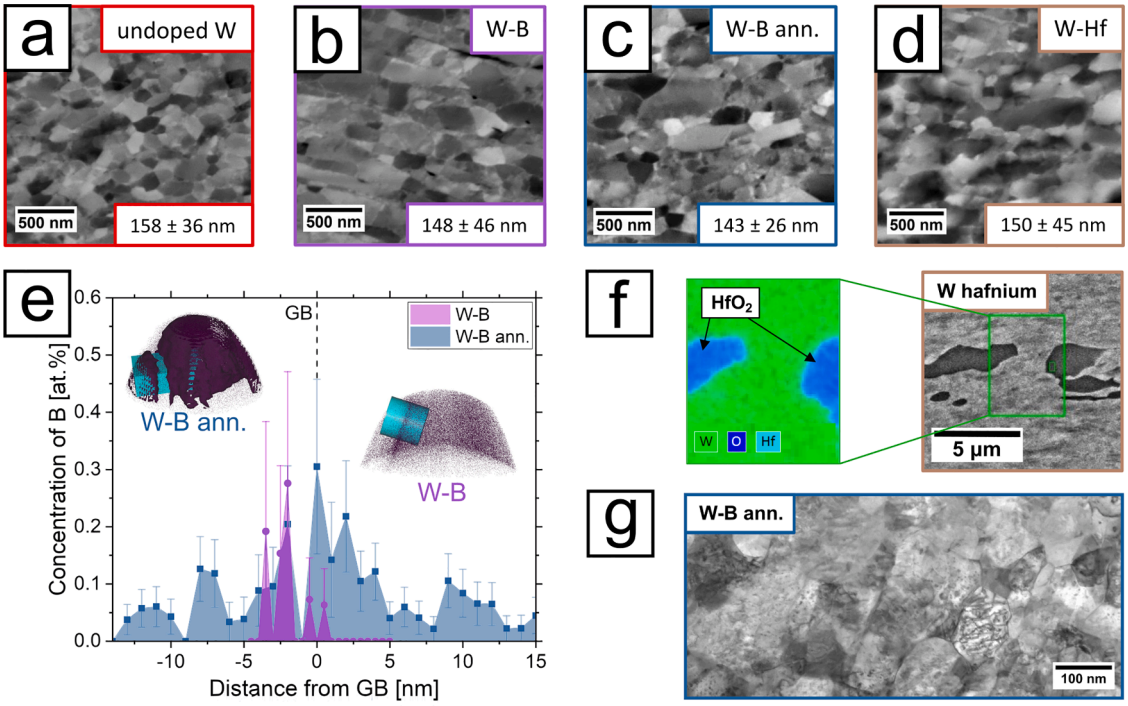

Fig. 2. Microstructure overview of investigated samples. SEM micrographs and indication of average grain sizes of (a) undoped W, (b) W-B, (c) annealed W-B and (d) W-Hf. (e) APT measurements of B content at GBs in W-B and annealed W-B, respectively. (f) EDX map showing HfO_2 particles in W-Hf samples. (g) STEM image of W-B ann. material.

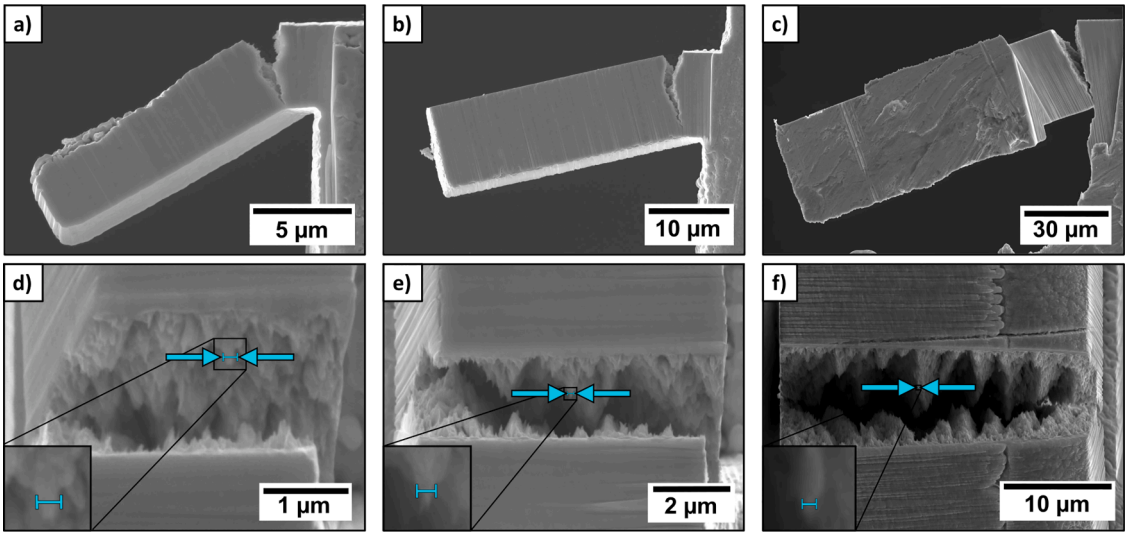

Fig. 3. SEM images of cantilever samples of different sizes and their fracture surfaces after testing. A small W-B cantilever (a,d), a medium sized W-B ann. cantilever (b,e) and a large undoped W cantilever (c,f). Cyan scale bars represent 150 nm, which is the approximate grain size for all materials.

the experimental J-Integral is a well-established option [37,61]:

$$J = \frac{K^2 \cdot (1-\upsilon^2)}{E} + \frac{\eta \cdot A_{pl}}{B \cdot (w-a_0)} \tag{2}$$

With υ being the Poisson's ratio and E the Young's Modulus of the material (for tungsten: $\upsilon = 0.28$ and $E = 410\ GPa$ [1]), η is a constant factor equal to 1.9 and A_{pl} is the plastic area under the force-displacement curve of the experiment (i.e. the plastic work). The stress intensity factor K is calculated via [36,37,59]:

$$K = \frac{F \cdot L_C}{B \cdot w^{3/2}} \cdot f\left(\frac{a}{w}\right) \tag{3}$$

with L_C being the distance between the point of loading and the notch (see Fig. 1).

The geometry factor $f\left(\frac{a}{w}\right)$ was calculated using FEM simulations [37] to be:

$$f\left(\frac{a}{w}\right) = 4 \cdot \frac{3 \cdot \left(\frac{a}{w}\right)^{0.5} \cdot \left(1.23 - \left(\frac{a}{w}\right) \cdot \left(1 - \frac{a}{w}\right)\right) \cdot \left(-6.09 + 13.96 \cdot \left(\frac{a}{w}\right) - 14.05 \cdot \left(\frac{a}{w}\right)^2\right)}{2 \cdot \left(1 + 2 \cdot \left(\frac{a}{w}\right)\right) \cdot \left(1 - \left(\frac{a}{w}\right)^{1.5}\right)} \tag{4}$$

where a represents the current crack length.

As is apparent in Eq. (4), it is essential for EPFM experiments that the

crack length is tracked throughout the whole experiment. This can either be done visually from the in-situ videos (manually or automatically with digital image correlation) or by frequent/continuous measurement of the sample stiffness throughout the experiment [62–67]. In this work, the stiffness of the cantilever is measured in regular steps by performing partial unloading segments during the experiment. Using the stiffness gained from the loading/unloading slopes, the current crack length can then be derived using the following FEM-based equation [62]:

$$\frac{a}{w} = 1 - 2.897\left(\frac{k}{k_0}\right) + 10.618\left(\frac{k}{k_0}\right)^2 - 23.620\left(\frac{k}{k_0}\right)^3 + 24.497\left(\frac{k}{k_0}\right)^4 - 9.600\left(\frac{k}{k_0}\right)^5 \quad (5)$$

Where k is the current cantilever stiffness and k_0 is the stiffness the cantilever would have without any crack. k_0 can be calculated from the first sample loading, where both the stiffness and the initial crack length a_0 are known [66,67].

The cantilevers were tested in-situ inside a LEO 982 SEM (Zeiss GmbH, Germany) using an UNAT-SEM indenter (Zwick GmbH & Co KG, Germany) equipped with a conductive diamond wedge indenter tip (Synton-MDP AG, Switzerland). The applied strain rate of the experiments was set to 0.001 s^{-1} at the notched region for all cantilevers.

Post-mortem images were taken with an SEM (Tescan Magna, Tescan Orsay Holding, Czech Republic).

3. Results

3.1. Interpretation of results

The analysis of EPFM experiments is not as straight-forward as for LEFM experiments, where fracture toughness values are determined via a simple equation and by measuring sample dimensions and the critical load. Instead, the J-Integral - crack extension (J-Δa) curve, also referred to as the R-curve, has to be calculated using the recorded force-displacement data in conjunction with Eqs. (2)–(5).

A representative example of such a J-Δa curve for a medium-sized undoped W cantilever is displayed in Fig. 4a. As apparent, one can fit two straight lines in the R-curve. The first, steeper line is commonly called “blunting line”. Here, crack extension occurs primarily through blunting of the crack tip, hence the name. The second, less steep regime represents actual crack growth or tearing. In the case of Fig. 4a this line increases with ongoing crack extension, indicating stable crack growth and an increasing crack growth resistance throughout the experiment. To receive a fracture toughness value from such a J-Δa curve, ASTM recommends to shift the blunting line to a crack extension of 0.2 mm and use the intersection of this parallel shifted line with the R-curve as a critical $J_{c0.2}$ value [59]. Obviously, this is not very helpful for small-scale tests, as the sample dimensions are considerably smaller than 0.2 mm. Therefore, this work relies on the initiation toughness J_i as a measure for fracture toughness, as has been used in microscale experiments before [37,68,69]. J_i represents the plastic energy needed to initiate regular crack growth and can be found at the intersection of the two fitted lines (Fig. 4a). The initiation toughness is especially well suited to characterize microsamples, as it is, contrary to the rest of the R-curve, geometry independent as long as certain specimen size requirements are fulfilled [46]. Another possible approach to make the evaluation of fracture toughness from J-Δa curves accessible to both the micro- and macroscale is to shift the blunting line by half of the crack tip opening displacement (CTOD) instead of 0.2 mm [38,62,70]. However, the measurement of CTOD is in many cases impractical. Yet, since CTOD was investigated in this work as well (see Section 4b), the fracture toughness deduced from this method was compared to the J_i values for all cantilevers showing stable crack growth. The difference between the values gained by the two methods was negligible for most samples, verifying the application of either method to assess fracture toughness values from J-Δa curves.

This kind of analysis can only be performed for stable crack growth and if the material shows R-curve behavior. Some samples presented within this work showed unstable crack growth, meaning the cantilever failed immediately by reaching a certain critical load and displacement after the blunting phase. A comparison of the load-displacement data of two experiments showing stable and unstable crack growth is shown in Fig. 4b and 4c, respectively. As is apparent, even for samples breaking in unstable manner some plastic deformation occurs before total failure. Since a J-Δa curve for such a sample would only consist of the blunting line, the J value at the failure point (J_c) is determined and utilized as a measure for fracture toughness for these samples. The comparison of J_i of the stable breaking samples to such critical J-Integral values J_c is in the opinion of the authors reasonable, as J_c is essentially equal to the initiation toughness of a material without increasing crack growth resistance, i.e. without R-curve behavior.

For a better comparability between fracture toughness values of commonly used LEFM experiments and the EPFM experiments utilized in this work, J_i and J_c values can be converted to $K_{J,i}$ and $K_{J,c}$ values, respectively, using the following equation [71]:

$$K_{J,i/c} = \sqrt{\frac{J_{i/c} \cdot E}{1 - \upsilon^2}} \quad (6)$$

within a plane strain assumption.

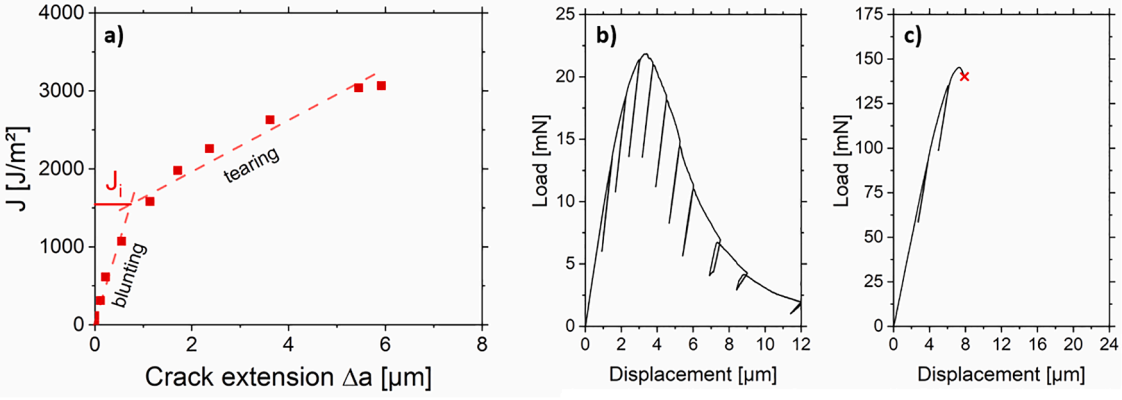

Fig. 4. a) Analysis of fracture toughness from J-Δa curves in EPFM experiments for a medium-sized undoped ufg W cantilever. (b, c) Representative load-displacement curves for stable (b, medium-sized cantilever) and unstable (c, large cantilever) crack growth in undoped ufg W.

3.2. Fracture toughness

Fig. 5 shows the fracture toughness of all tested samples. J_i is shown for samples that exhibit stable crack growth (open symbols), whereas J_c is shown for samples that fail in an unstable manner (solid symbols). It is immediately apparent that cantilevers of the same material but different sample dimensions can show vastly different toughness values and crack growth behavior, indicating the presence of a size effect and questioning the validity of some experiments, as will be further elaborated in the discussion section. Note that one large W-Hf cantilever (marked with "*") contained a micron sized oxide particle at the fracture surface directly beneath the initial notch, suggesting that the measured fracture toughness of this specimen is an underestimation of the actual material toughness). The relative error in J_i and J_c was calculated following the principle of propagation of uncertainty and assuming a possible measurement error of 1 pixel for each sample dimension. It amounts to values between 0.5 and 1% for all tested samples. As this relative error is very small, we refrain from the use of error bars in Fig. 5 and the following figures, as they would not be visible.

The small cantilevers (3 × 3 × 10 μm, triangle symbols in Fig. 5) of all tested materials show stable crack growth and similar toughness values of around 300–700 J/m^2 or 12–18 MPa$\sqrt{m}$. The medium-sized cantilevers (8 × 8 × 30 μm, square symbols in Fig. 5) display less uniform behavior. While some samples exhibit stable crack growth and very high toughness values of up to over 2000 J/m^2 (30 MPa$\sqrt{m}$), others show unstable failure and toughness values of around 1000 J/m^2 (20 MPa$\sqrt{m}$). It is interesting to note, that the materials that show unstable failure (W-B and W-B ann.) were found in microcantilever bending tests to have a higher bending strength than the undoped W and W-Hf material [35]. For the larger cantilevers (star symbols in Fig. 5), all samples showed unstable crack growth behavior. The fracture toughness was measured to be 1040 J/m^2 (21.5 MPa$\sqrt{m}$) for the undoped W sample and 1860 J/m^2 (28.8 MPa$\sqrt{m}$) as well as 1480 J/m^2 (25.6 MPa$\sqrt{m}$) for the W-Hf samples, respectively.

All fractured surfaces show clear signs of intercrystalline failure (delamination) with a share of ductile failure (shearing), regardless of material, cantilever dimensions or stability of crack growth. It is clearly evidenced in Fig. 3 that the size of characteristic features of the fracture surfaces correspond well with the approximate grain size of 150 nm (cyan scale bars) for all sample dimensions. Moreover, previous work on doped and undoped ufg W [35] used EBSD to confirm the intercrystalline failure mode of this material.

4. Discussion

4.1. Validity of fracture experiments

Following the results of micro- and meso-scale fracture mechanical experiments, some remarks on the validity of the experiments are in order. Given the comparably large sample dimensions, it is safe to assume that the large cantilevers of undoped and Hf-doped ufg W represent valid EPFM experiments. These cantilevers, together with the medium-sized W-B ann. cantilever and one W-B cantilever, show unstable failure and similar toughness values. This raises the question whether the instability of crack growth might be an indicator for a valid EPFM experiment on ufg W.

The validity criterion of EPFM *J*-Integral experiments is commonly given as:

$$B,\ (w-a_0)\ >\ c\ \frac{J_Q}{\sigma_y} \tag{7}$$

Where J_Q is the conditional *J*-Integral fracture toughness gained from the experiment, σ_y is the yield stress of the material and *c* is a pre-factor. Values ranging from 10 to 50 are reported in literature for this pre-factor [37,38,40] and the official standard by ASTM gives a value of 10 [71].

Fig. 6 shows the fracture toughness of all tested samples, this time displayed against the rearranged validity criterion of Eq. (7) on the x-axis. The smaller dimension among sample thickness *B* and ligament length $(w-a_0)$ is used for each specimen. The yield strength is taken from bending experiments performed on the same material in [35]. Of course this is not the same value as a yield strength gained from tensile tests, which is why some points might not be placed with highest accuracy, but it serves as a good estimate and provides comparability between the samples. It should be noted that the yield strength is the same for all tested cantilever sizes. It has been shown before for different ufg metals, including W, that the grain size regime of 100–200 nm does not lead to size effects regarding strength or plastic deformation on the studied μm scale, as a sufficient number of grains span the sample cross-section [72–74]. $J_{c,true}$ represents the valid J-Integral fracture toughness of the material, which is gained from the experiments with the largest sample dimensions for each material (as they are assumed to represent valid EPFM experiments). These experiments all displayed unstable crack growth. The term $\frac{J}{\sigma_y}$ is proportional to CTOD and plastic zone size [46]. Therefore, the x-axis in the graph represents the ratio of sample dimensions to plastic zone size or the pre-factor *c* in the validity

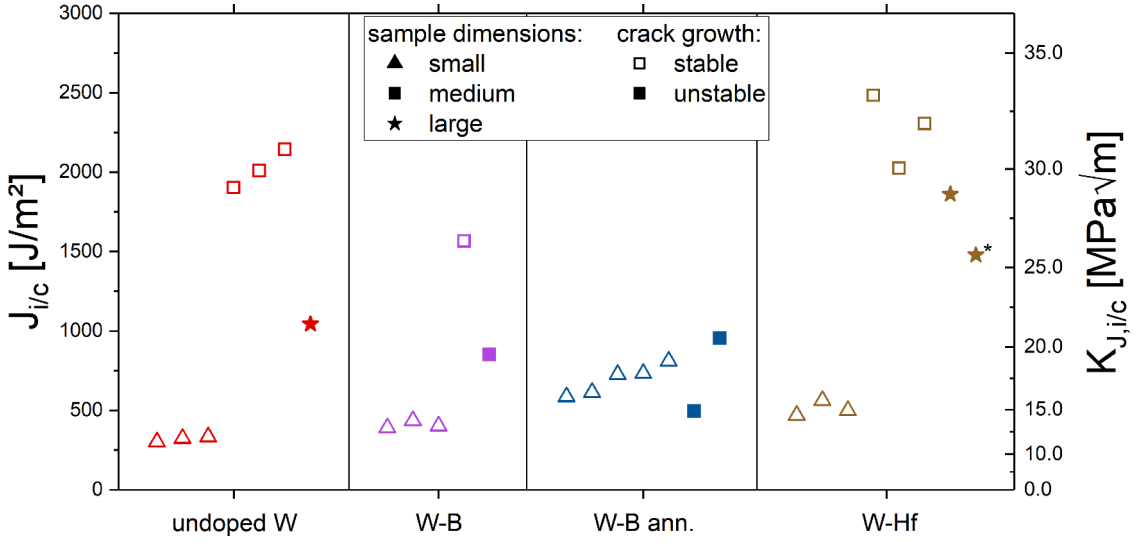

Fig. 5. Fracture toughness (J_i or J_c) of all tested cantilevers gained from EPFM experiments on all investigated ufg W materials. Open symbols represent experiments with stable crack growth, solid symbols display unstable failure. (*: cantilever contained oxide particle on fracture surface just below initial notch).

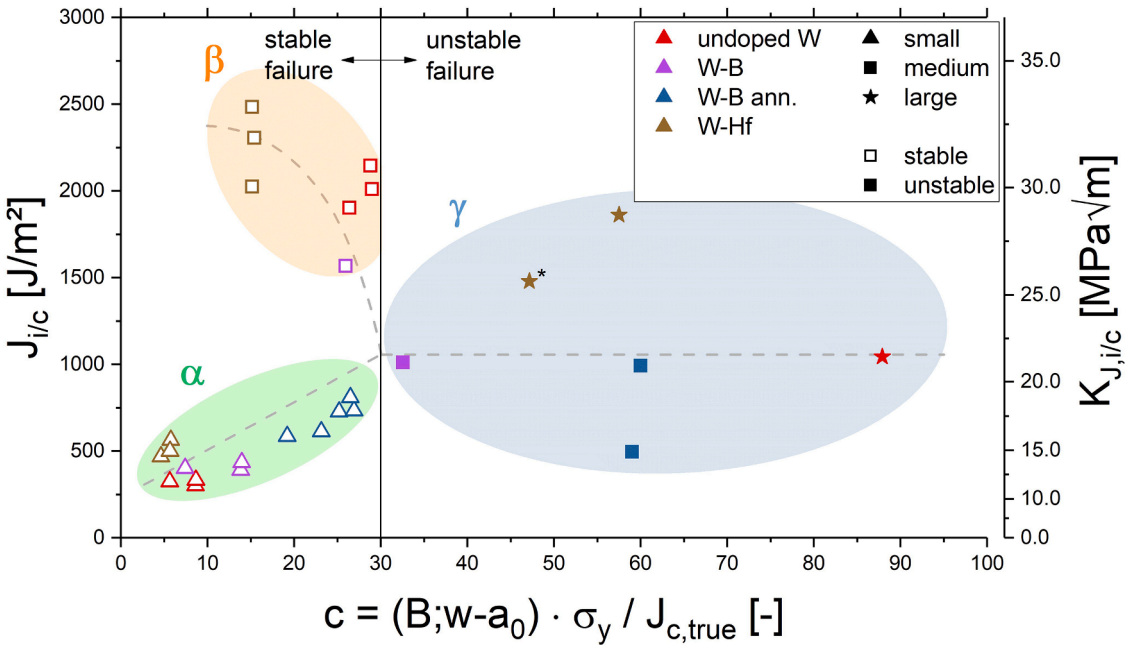

Fig. 6. Fracture toughness (J_i or J_c) of all tested cantilevers over the smallest dimension of the cantilever times yield strength divided by valid fracture toughness of the material. The x-value is proportional to the ratio of sample dimension to plastic zone size in front of the crack tip and resembles c in Eq. (7). For further analysis, the fracture samples are classified in regimes "α", "β" and "γ". (*: cantilever contained oxide particle on fracture surface just below initial notch).

criterion of Eq. (7).

It is apparent in Fig. 6 that above a certain x-value (in this concrete case ~30) all samples fail in an unstable manner and show comparable fracture toughness values (regime "γ"). This strongly suggests that above this value the experiments are valid and the measured fracture toughness equals the real, size independent, fracture toughness of the material. Naturally, the largest cantilevers fulfill this condition easily. For the medium-sized cantilevers, only the higher strength materials (W-B ann. and one out of two W-B) fulfill this condition, as the higher yield strength leads to a smaller plastic zone within the cantilever. Here it is worth noting that the W-B material has one cantilever on either side of the validity line. This is because the cantilever sample on the left side had slightly smaller dimensions than the sample on the right side. The medium-sized cantilevers made of softer material and all small cantilevers cannot fulfill the validity criterion ($c > 30$), but they show vastly different fracture toughness values. While the smaller samples underestimate the real fracture toughness (regime "α"), the invalid medium-sized cantilevers overestimate it (regime "β"). Before an explanation for this peculiar behavior can be attempted, a more detailed analysis of the fracture behavior is required and will be performed next.

4.2. Analysis of the crack tip opening displacement

To provide further information on fracture behavior and apparent toughness, another widely used option to measure fracture toughness within EPFM was utilized: the crack tip opening displacement (CTOD). It was proven before that both the J-Integral and CTOD can be used to measure the correct fracture toughness of EPFM samples and are connected via [37,71,75,76]:

$$CTOD = d_n \frac{J}{\sigma_y} \tag{8}$$

Where d_n is the Shih factor, which is equal to 0.78 for plane strain conditions and a non-hardening material.

Given the in-situ nature of the experiments in this work, the CTOD at crack growth initiation ($CTOD_i$, for stable crack growth) or the critical CTOD before failure ($CTOD_c$, for unstable crack growth) can be measured directly from the videos recorded during the experiments. Due to the fast scanning speed of the SEM during the tests, the resolution of the images is limited, which is why the CTOD was measured multiple times for each sample to provide an accurate average value. The results of the CTOD measurement can be seen in Fig. 7a. The small cantilever samples exhibit a similar trend than in Fig. 6, showing smaller CTOD values with a linear increasing trend. Fig. 7b shows the J-Integral calculated from CTOD results using Eq. (8) and a Shih factor of 0.78. While the J-values of the unstable failing samples are very similar to the J-values gained from Eqs. (2)–(5) (with the exception of the annealed W-B sample, see also Fig. 10a), the values of the stable failing samples are rather different and show a dissimilar, more linear trend. It should be mentioned that, in ductile materials, the CTOD at the surface is usually smaller (before crack growth initiation) or larger (after crack growth initiation) than the "valid" CTOD in the midsection of the sample [77]. However, since the values of J_{CTOD} and J_c are so similar for the unstable failing samples, it is assumed that for the current failure mode (i.e. a complex mixture of intercrystalline and ductile fracture), the CTOD at the surface and within the sample are comparable.

4.3. The role of sample dimensions on perceived fracture toughness

When considering some of the standard validity criterions used in fracture mechanics, e.g. Eqs. (1) and (7), a common misconception which can arise is that the two critical sample dimensions, i.e. the ligament length $w - a_0$ and the sample thickness B, each have a similar effect on the fracture behavior of the material, as the same criterion is applied to either measurement. In reality, the implications of the two dimensions are vastly different. The ligament length (in combination with the plastic zone size) determines if the test specimen exhibits small scale yielding, large scale yielding or failure through plastic collapse, and therefore governs the validity of applying LEFM or EPFM concepts. The sample thickness, on the other hand, influences the stress state in front of the crack tip. A large sample thickness leads to predominantly plane strain conditions and consequently a high stress triaxiality at the crack tip. On the surface of the sample, plane stress conditions prevail. It can be easily deduced that with decreasing sample thickness the influence of this plane-stress dominated region increases, leading to lower

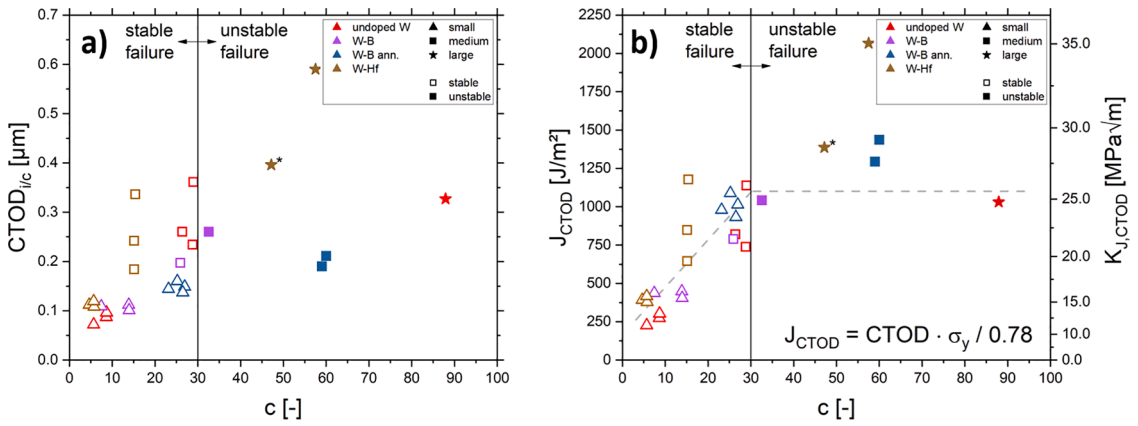

Fig. 7. (a) Measured crack tip opening displacement at crack growth initiation ($CTOD_i$) or before failure ($CTOD_c$) for all tested samples. (b) J-Integral fracture toughness based on CTOD measurements. (*: cantilever contained oxide particle on fracture surface just below initial notch).

overall stress triaxiality in the test specimen [75,78,79]. It has to be mentioned that strictly speaking, a specimen fulfilling the ligament length criterion but not the thickness criterion still represents a valid fracture mechanical experiment. However, as the influence of the plane stress condition increases, the measured fracture toughness becomes thickness dependent. This thickness dependent toughness increases with decreasing B, as long as the process zone stays small compared to the sample thickness [46]. Therefore, it is common practice to determine the sample size independent "plane strain fracture toughness", that can only be measured in samples thick enough to show predominantly plane strain conditions and high stress triaxiality throughout the crack front. In commonly used macro-sized LEFM experiments, one hardly ever measures such a thickness dependent fracture toughness, as the criterion is very strict (Eq. (1)) and it is much more likely to run into validity issues regarding the ligament length criterion (assuming ligament length and sample thickness are in the same order of magnitude) [75]. In EPFM experiments, however, where sample dimensions are smaller and/or plastic zone sizes are large, it can become a lot more likely to measure thickness dependent fracture toughness, as the ligament length criterion is far more forgiving and the influence of the sample thickness on stress triaxiality is the same as in LEFM experiments.

When the apparent fracture toughness is plotted against the sample thickness B (Fig. 8), one can visualize a similar trend in all ufg W variants. Small samples show a low fracture toughness, stable failing medium-sized samples display a higher fracture toughness, and unstable breaking samples fall into the regime of a constant, thickness-independent fracture toughness. It is interesting to note that the peak of high toughness values increases with increasing plastic zone size (ratio of $\frac{J}{\sigma_y}$) and also moves towards larger sample thicknesses. The increase of fracture toughness for the samples in region "β" in Fig. 6 (peak region in Fig. 8) can be explained by a significant influence of plane stress conditions leading to the assessment of a thickness-dependent toughness. The results from CTOD analysis confirm this, as the J_{CTOD} values are significantly lower than the J_c values for regime "β" samples. This is because the Shih factor d_n of 0.78 is only valid for plane strain conditions and has to be adapted if samples show increased plane stress influence and lower triaxiality [76]. As only the unstable failing samples (region "γ") display comparable values of J_{CTOD} and J_c, this suggests that predominantly plane strain conditions are only present in these samples, while all others exhibit primarily plane stress influenced conditions,

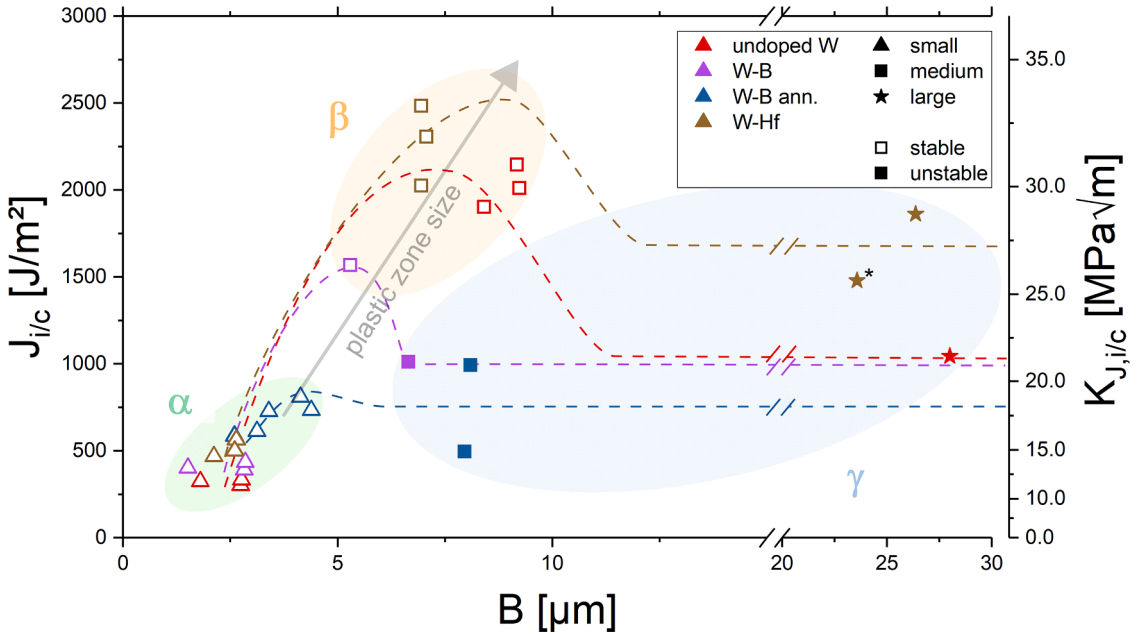

Fig. 8. Fracture toughness (J_i or J_c) of all tested cantilevers over sample thickness B. For each individual material the apparent fracture toughness shows a similar trend with increasing thickness. Dashed lines represent a guide for the eye. (*: cantilever contained oxide particle on fracture surface just below initial notch).

which would require an adaption of the Shih factor for more detailed analysis.

However, the decrease in toughness of the thinnest samples within region "α" cannot be reasoned by such a thickness effect. Since no significant plastic deformation of the sample was observed in the in-situ experiments, plastic collapse of the ligament [60], i.e. the breakdown of large-scale yielding conditions, can be ruled out as well. Given the fact that all these samples are small cantilever specimen and that the ratio of sample dimensions to plastic zone size is comparable to some region "β" samples, it is expected that these specimen are increasingly influenced by sample geometry and less by material properties. It is well known that a (cantilever) bending sample experiences a stress and strain gradient, with tensile stress states on one and compressive stress states on the other side. It can be followed easily that such a gradient will be a lot steeper for a smaller specimen. By introducing a crack/notch to the specimen, the stress field in front of the crack tip, as well as the fracture process zone, are influenced by both the crack tip itself and the bending stress gradient field. The fracture process zone is commonly defined as the region where micromechanical processes occur that contribute to crack propagation [46,75]. This rather loose definition ranges from pore formation and coalescence in ductile materials, dislocation emission from the crack tip and their propagation, crack bifurcation and tunneling in semi-brittle materials to the breaking of individual atomic bonds in ideally brittle materials. In ductile materials this fracture process zone is typically in the order of a few CTOD, yet it might be even larger in the case of a mixed ductile and intercrystalline fracture, as is the case in the present study [46]. It seems from the data in Figs. 6 and 8 (regime "α") that once the fracture process zone reaches past the neutral fiber of the bending cantilever, the compressive part of the stress and strain gradient influences the fracture process zone and impedes its further expansion. As a consequence, stresses can be dissipated less effectively from the crack tip and failure occurs at lower loads and fracture toughness values. This also explains the low CTOD results for the smaller samples in Fig. 7, as a restricted fracture process zone leads to a smaller CTOD. A similar argument can be made for a restriction in plastic zone size (and therefore amount of plastic deformation), leading to lower fracture toughness through less effective dissipation of crack driving force.

As an accurate assessment of the fracture process zone is near impossible, a closer analysis of the plastic zone size will be attempted next instead. FEM simulations were performed using the free CalculiX 2.17 solver [80], on three representative cantilever sizes: small, medium and large. The 2-dimensional simulations were conducted using 8-node quadrilateral plane strain elements (CPE8) with linear elastic isotropic material assumptions. As the aim was to investigate the opening stress behavior over the whole crack growth direction including the bending gradient the common use of crack tip elements with specific side-node positions (to obtain an element corner singularity) was neglected. The simulated stresses σ_{xx} in front of the crack tip (at the load of crack growth initiation or the transition from blunting to tearing) are displayed in Fig. 9. By considering the yield strength of undoped ufg W known from bending tests (~3.28 GPa) [35], one can estimate the size and shape of the plastic zone in these cantilever samples as the region where the simulated stress equals or exceeds the yield strength. As displayed in Fig. 9, this plastic zone (blue shape) resembles the "butterfly" shape commonly encountered in fracture experiments. This can now be compared to common plastic zone models, such as the Irwin model, which describes the (plane strain) plastic zone size in a semi-infinite body as such [75,81]:

$$r_{pl} = \frac{1}{6\pi}\left(\frac{K}{\sigma_y}\right)^2 \tag{9}$$

The plastic zone calculated after Irwin is about 2.3 μm big for undoped ufg W and is displayed as a representative green circle in Fig. 9. It is immediately apparent that the size of the plastic zone inside the small cantilever, calculated using the stress field provided by FEM, is immensely restricted compared to the plastic zone the material would experience in a semi-infinite tension sample (Irwin model). This restriction is less severe in the medium-sized cantilever and almost non-existent in the large sample. It should be mentioned that, due to the simplicity of both the FEM simulation and the Irwin model, the results in Fig. 9 should not be used for quantitative assessment of the plastic zone size (or the margin of the restriction thereof), but rather as an attempt to qualitatively explain the drop due to the strongly reduced energy dissipation in the small samples with consequently low fracture toughness for very small cantilever specimen. The stress field simulated by FEM is representing plane strain conditions, not taking into account any thickness effects. Note that 3-dimensional strain gradient plasticity FEM [82–84] or cohesive zone models [85,86] could capture the effect of the bending gradient on the plastic zone and fracture toughness more accurately. However, these demanding simulation approaches are well beyond the scope of this work, but an interesting option for future detailed investigation of the presented or similar experiments.

To summarize, the apparent fracture toughness values in Fig. 6 can be explained as such:

- Samples that are large enough exhibit unstable fracture and more or less constant fracture toughness values (region "γ"). They fulfill the thickness criterion of predominantly plane strain conditions in front of the crack tip and can be seen as valid "plane strain fracture toughness" values. These specimen fully describe the sample size independent fracture behavior of the materials. The fact that all these specimen show unstable crack propagation is further evidence of predominantly plane strain conditions, as it is known that plane stress influenced conditions (such as in region "β") promote R-curve behavior and stable crack growth [46]. Given the large sample dimensions, no significant influence of the bending gradient on the

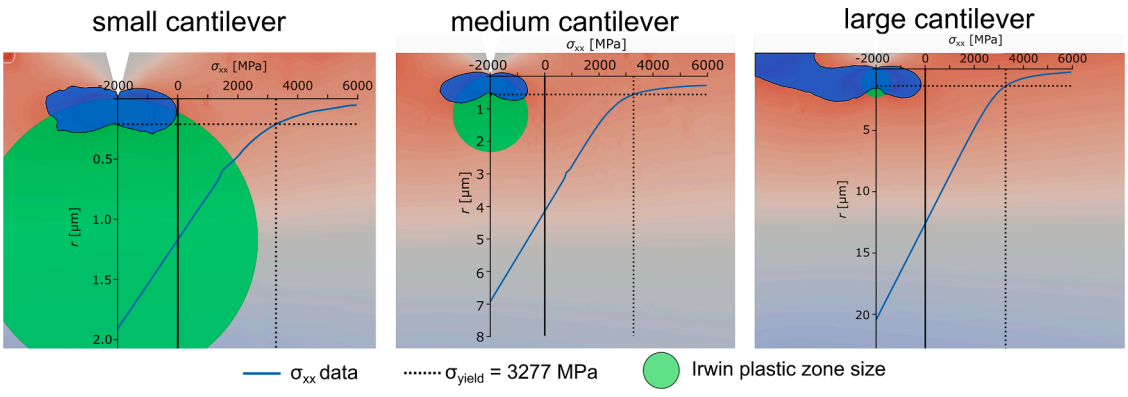

Fig. 9. FEM simulations showing the influence of the bending stress gradient on the size of the plastic zone, compared to the classic Irwin model, for undoped ufg W.

specimen stress and strain distribution, and therefore plastic zone size, are expected.

- For the medium-sized cantilever specimen that show stable crack growth and high fracture toughness values (region "β"), the influence of the sample thickness cannot be underestimated. It is expected that for these specimen marked with "β" in Fig. 6, an increased influence of plane stress conditions and, consequently, a lower overall stress triaxiality within the process zone are present. This results in a thickness dependent and higher perceived fracture toughness compared to predominantly plane strain conditions. For such samples, the crack will most likely start propagating in the center of the specimen when the plane strain fracture toughness value is reached, while the increase in apparent fracture toughness stems from the surface near regions where crack growth lags behind [46]. Compared to the increase in plastic zone size from the predominantly plane stress affected stress state, the bending stress gradient in these samples is expected to only have a negligible influence on the plastic zone, as the fracture process zone does likely not extend past the neutral fiber. Note also that region "β" for the annealed W-B material is almost non-existent. As this material has an extremely high strength, and hence small plastic zone, the geometrical influence of the bending gradient dominates over the increasing plane stress conditions, which is why we categorized even the data points with slightly higher toughness (small "hump" in the trending line) under regime "α", i.e. severely influenced by the bending gradient.
- The small cantilever samples marked in region "α" experience a significant influence from the bending strain gradient on the fracture process zone. Additionally, the impact of the bending stress on the stress field in front of the crack tip is shown by FEM simulations to reduce the size of the plastic zone substantially, as compared to the plastic zone the material would form in a semi-infinite sample (Irwin approximation; see Fig. 9). As both the plastic zone and fracture process zone are being restricted, stresses can be dissipated less effectively from the crack tip, leading to earlier failure and a lower apparent fracture toughness. In these small samples, the plastic zone and fracture process zone get severely restricted, which clearly outweighs the thickness effect of predominantly plane stress conditions. The larger the sample or harder the material gets, the less the influence of this strain gradient becomes, explaining the slight increase of toughness for the small samples in Fig. 6.

4.4. The effect of doping elements on fracture toughness of ufg W

Naturally, only the experiments to the right of the line in Fig. 6 (regime "γ") show the size-independent fracture toughness and can thus be used to compare the different materials with each other. Fig. 10a displays these values (converted to K_J values using Eq. (6)) gained from J-Integral and CTOD analysis for all investigated samples. For materials with multiple valid fracture experiments (W-B ann. and W-Hf), the mean toughness values are displayed. Overall, the fracture toughness of the ufg W materials show remarkably high values of around 21 MPa$\sqrt{m}$, clearly outperforming single-crystalline and other ufg W samples, for which values of around 6–12 MPa$\sqrt{m}$ are reported in literature [18,37,43,68,87]. Previous work on bulk HPT-processed ufg W by Faleschini et al. reports similar fracture toughness [18,19]. The RT-toughness values measured in this work are even higher than the fracture toughness of cg W above the BDTT [43,87], therefore clearly fulfilling the application requirements in nuclear fusion reactors [2–4], at least for the given testing direction.

The agreement between the fracture toughness measured by the two different methods is given for all materials, except the annealed W-B sample. As the measurement of the CTOD from in-situ images is more prone to errors (a measurement error of 1 pixel (~30 nm) would result in a fracture toughness error of about 2 MPa$\sqrt{m}$, a measurement error of 3 pixel (~90 nm) would misevaluate the fracture toughness by about 5 MPa$\sqrt{m}$), the more conservative stance is taken and the lower toughness gained from J-Integral analysis is assumed to be the true fracture toughness for this material. However, given the immense strength increase that was discovered in bending tests on this material [35], this slight decrease in toughness to 17 MPa$\sqrt{m}$ is more than being compensated for. While the B-doped and unannealed sample shows a similar fracture toughness to the undoped material, the fracture toughness of the ufg W material doped with Hf shows a significant improvement to values of 27-28 MPa$\sqrt{m}$. This is not particularly surprising, as Hf was the only doping element that was able to improve bending ductility in [35] and, especially for ufg and nanocrystalline materials, ductility and fracture toughness are closely interlinked due to the intercrystalline nature of failure. The extent of improvement of fracture toughness by Hf doping is, however, astounding. As deduced in [35], Hf does not strengthen the GBs in W directly, but indirectly by removing oxygen from the boundaries and binding them in HfO_2 oxides (see Fig. 2f). This seems to be rather effective, given the outstanding improvements in bending ductility and now fracture toughness.

Fig. 10b shows average bending strength (from [35]) and fracture toughness of each investigated material and the ufg W sample fabricated by Faleschini et al. [19] for comparison. Hohenwarter et al. [21] introduced the product of strength and toughness as an easy and accessible measure for damage tolerance of materials. The dashed isolines in Fig. 10b represent this product. It can be seen that all doped and annealed variants show a clear improvement of damage tolerance

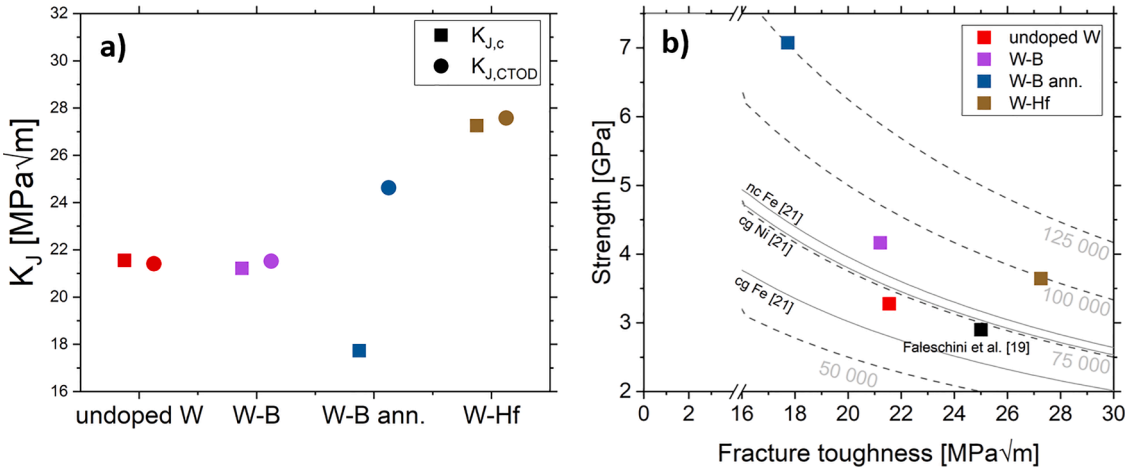

Fig. 10. (a) Comparison of fracture toughness values (K_J) gained by J-Integral and CTOD analysis. (b) Average bending strength against valid fracture toughness ($K_{J,c}$) of all investigated ufg W materials. Dashed isolines represent the product of strength and toughness in (MPa)$^2\sqrt{m}$.

compared to the undoped ufg W sample, with W-Hf (~ 100 000 $(MPa)^2\sqrt{m}$) and W-B ann. (~ 125 000 $(MPa)^2\sqrt{m}$) demonstrating the highest values and even outperform coarse grained Ni, coarse grained Fe and nanocrystalline Fe [21] (solid isolines in Fig. 10b), respectively.

5. Conclusion

In this work, through the application of small-scale EPFM experiments on doped and undoped ufg W, two major conclusions can be drawn:

- EPFM experiments at the microscales for semi-brittle materials such as ufg W (and for ductile materials) have to be performed with great caution and with the effects of sample dimensions on the apparent fracture toughness in mind. For especially small cantilever samples the effects of the bending strain gradient on the fracture process zone, as well as the bending stress gradient on the crack tip stress field and, consequently, the plastic zone size, have to be considered. A severely restricted fracture process zone and plastic zone can lead to lower apparent fracture toughness values. If the sample dimensions are sufficiently large to avoid being severely affected by the bending gradient, one has to be careful that the sample is thick enough to not experience increasingly plane stress affected conditions, which can lead to a sample size dependent and higher apparent fracture toughness. A safe pre-factor of at least 30 in Eq. (7) (ratio of smallest sample dimension to plastic zone size), thus stricter than in macroscopic standards, is recommended for the correct evaluation of a size-independent fracture toughness.
- The sample size-independent fracture toughness of undoped W can be increased from ~20 $MPa\sqrt{m}$ to almost 30 $MPa\sqrt{m}$ with the addition of Hf as a doping element. The addition of B maintains the toughness, while an additional heat treatment can lead to a slight decrease in fracture toughness but immensely increases the strength of the material, improving the overall damage tolerance of ufg W.

The insights from this work are expected to be valuable for the application of ufg W in extreme environments, such as nuclear fusion technology, and for the potential future development of a small-scale fracture test routine for control samples in harsh conditions and for limited materials, as well as for scientists and material research centers dealing with such issues, such as the International Fusion Materials Irradiation Facility (IFMIF).

Declaration of Competing Interest

The authors declare that they have no known competing financial interests or personal relationships that could have appeared to influence the work reported in this paper.

Acknowledgements

Funding by the European Research Council (ERC) under grant number 771146 (TOUGHIT) is greatly acknowledged. The authors thank Simon Doppermann and Benjamin Seligmann for help with material and sample preparation.

References

[1] E. Lassner, W.-.D. Schubert, Tungsten. Properties, Chemistry, Technology of the Element, Alloys, and Chemical Compounds, Kluwer Academic /Plenum Publishers, New York, 1999, https://doi.org/10.1007/978-1-4615-4907-9.

[2] M. Rieth, D.E.J. Armstrong, B. Dafferner, S. Heger, A. Hoffmann, M. Hoffmann, U. Jäntsch, M. Rohde, T. Scherer, V. Widak, H. Zimmermann, Tungsten as a structural divertor material, Adv. Sci. Technol. 73 (2010) 11–21, https://doi.org/10.4028/www.scientific.net/AST.73.11.

[3] S. Wurster, N. Baluc, M. Battabyal, T. Crosby, J. Du, C. Garcia-Rosales, A. Hasegawa, A. Hoffmann, A. Kimura, H. Kurishita, R.J. Kurtz, H. Li, S. Noh, J. Reiser, J. Riesch, M. Rieth, W. Setyawan, M. Walter, J.-.H. You, R. Pippan, Recent progress in R&D on tungsten alloys for divertor structural and plasma facing materials, J. Nucl. Mater. 442 (2013) 181–189.

[4] M. Rieth, S.L. Dudarev, S.M.G. De Vicente, J. Aktaa, T. Ahlgren, S. Antusch, D.E. J. Armstrong, M. Balden, N. Baluc, M. Barthe, W.W. Basuki, M. Battabyal, C. S. Becquart, D. Blagoeva, H. Boldyryeva, J. Brinkmann, M. Celino, L. Ciupinski, J. B. Correia, A. De Backer, C. Domain, E. Gaganidze, C. Garcia-Rosales, J. Gibson, M. R. Gilbert, S. Giusepponi, B. Gludovatz, H. Greuner, K. Heinola, T. Höschen, A. Hoffmann, N. Holstein, F. Koch, W. Krauss, H. Li, S. Lindig, J. Linke, C. Linsmeier, P. López-ruiz, H. Maier, J. Matejicek, T.P. Mishra, M. Walter, T. Weber, T. Weitkamp, S. Wurster, M.A. Yar, J.H. You, A. Zivelonghi, Recent progress in research on tungsten materials for nuclear fusion applications in Europe, J. Nucl. Mater. 432 (2013) 482–500, https://doi.org/10.1016/j.jnucmat.2012.08.018.

[5] J.W. Davis, V.R. Barabash, A. Makhankov, L. Plöchl, K.T. Slattery, Assessment of tungsten for use in the ITER plasma facing components, J. Nucl. Mater. 263 (1998) 308–312.

[6] R. Neu, R. Dux, A. Kallenbach, T. Pütterich, M. Balden, J.C. Fuchs, A. Herrmann, C. F. Maggi, M. O'Mullane, R. Pugno, I. Radivojevic, V. Rohde, A.C.C. Sips, W. Suttrop, A. Whiteford, Tungsten : an option for divertor and main chamber plasma facing components, Nucl. Fusion. 45 (2005) 209–218, https://doi.org/10.1088/0029-5515/45/3/007.

[7] C. Ren, Z.Z. Fang, M. Koopman, B. Butler, J. Paramore, S. Middlemas, Methods for improving ductility of tungsten - a review, Int. J. Refract. Metals Hard Mater. 75 (2018) 170–183, https://doi.org/10.1016/j.ijrmhm.2018.04.012.

[8] L. Yang, K. Zhang, M. Wen, Z. Hou, C. Gong, X. Liu, C. Hu, X. Cui, W. Zheng, Highly hard yet toughened bcc-W coating by doping unexpectedly low B content, Sci. Rep. 7 (2017) 1–8, https://doi.org/10.1038/s41598-017-09807-9.

[9] M.J. Pfeifenberger, V. Nikolic, S. Zak, A. Hohenwarter, R. Pippan, Evaluation of the intergranular crack growth resistance of ultrafine grained tungsten materials, Acta Mater 176 (2019) 330–340, https://doi.org/10.1016/j.actamat.2019.06.051.

[10] J. Reiser, J. Hoffmann, U. Jäntsch, M. Klimenkov, S. Bonk, C. Bonnekoh, A. Hoffmann, T. Mrotzek, M. Rieth, Ductilisation of tungsten (W): on the increase of strength AND room-temperature tensile ductility through cold-rolling, Int. J. Refract. Met. Hard Mater. 64 (2017) 261–278, https://doi.org/10.1016/j.ijrmhm.2016.10.018.

[11] C. Bonnekoh, A. Hoffmann, J. Reiser, The brittle-to-ductile transition in cold rolled tungsten: on the decrease of the brittle-to-ductile transition by 600K to − 65°C, Int. J. Refract. Met. Hard Mater. 71 (2018) 181–189, https://doi.org/10.1016/j.ijrmhm.2017.11.017.

[12] C. Bonnekoh, J. Reiser, A. Hartmaier, S. Bonk, A. Hoffmann, M. Rieth, The brittle-to-ductile transition in cold-rolled tungsten sheets: the rate-limiting mechanism of plasticity controlling the BDT in ultrafine-grained tungsten, J. Mater. Sci. 55 (2020) 12314–12337, https://doi.org/10.1007/s10853-020-04801-5.

[13] C. Bonnekoh, U. Jäntsch, J. Hoffmann, H. Leiste, A. Hartmaier, D. Weygand, A. Hoffmann, J. Reiser, The brittle-to-ductile transition in cold rolled tungsten plates: impact of crystallographic texture, grain size and dislocation density on the transition temperature, Int. J. Refract. Met. Hard Mater. 78 (2019) 146–163, https://doi.org/10.1016/j.ijrmhm.2018.09.010.

[14] J. Riesch, J. Almanstötter, J.W. Coenen, M. Fuhr, H. Gietl, Y. Han, T. Höschen, C. Linsmeier, N. Travitzky, P. Zhao, R. Neu, Properties of drawn W wire used as high performance fibre in tungsten fibre-reinforced tungsten composite, IOP Conf. Ser. Mater. Sci. Eng. (2016) 139, https://doi.org/10.1088/1757-899X/139/1/012043.

[15] J. Riesch, A. Feichtmayer, M. Fuhr, J. Almanstötter, J.W. Coenen, H. Gietl, T. Höschen, C. Linsmeier, R. Neu, Tensile behaviour of drawn tungsten wire used in tungsten fibre-reinforced tungsten composites, Phys. Scr. (2017) 2017, https://doi.org/10.1088/1402-4896/aa891d.

[16] V. Nikolić, J. Riesch, R. Pippan, The effect of heat treatments on pure and potassium doped drawn tungsten wires: part I - Microstructural characterization, Mater. Sci. Eng. A 737 (2018) 422–433, https://doi.org/10.1016/j.msea.2018.09.027.

[17] V. Nikolić, J. Riesch, M.J. Pfeifenberger, R. Pippan, The effect of heat treatments on pure and potassium doped drawn tungsten wires: part II – Fracture properties, Mater. Sci. Eng. A 737 (2018) 434–447, https://doi.org/10.1016/j.msea.2018.09.029.

[18] M. Faleschini, H. Kreuzer, D. Kiener, R. Pippan, Fracture toughness investigations of tungsten alloys and SPD tungsten alloys, J. Nucl. Mater. 367–370 (2007) 800–805, https://doi.org/10.1016/j.jnucmat.2007.03.079.

[19] M. Faleschini, D. Kiener, W. Knabl, R. Pippan, Fracture Toughness investigations of tungsten alloys and severe plastic deformed tungsten alloys, in: Proceedings of the 16th International Plansee Seminar, 2005, pp. 701–711.

[20] R. Pippan, A. Hohenwarter, The importance of fracture toughness in ultrafine and nanocrystalline bulk materials, Mater. Res. Lett. 4 (2016) 127–136, https://doi.org/10.1080/21663831.2016.1166403.

[21] A. Hohenwarter, R. Pippan, Fracture and fracture toughness of nanopolycrystalline metals produced by severe plastic deformation, Philos. Trans. R. Soc. A 373 (2015), 20140366, https://doi.org/10.1098/rsta.2014.0366.

[22] A. Pineau, A.A. Benzerga, T. Pardoen, Failure of metals I: brittle and ductile fracture, Acta Mater. 107 (2016) 424–483, https://doi.org/10.1016/j.actamat.2015.12.034.

[23] A. Pineau, A. Amine Benzerga, T. Pardoen, Failure of metals III: fracture and fatigue of nanostructured metallic materials, Acta Mater. 107 (2016) 508–544, https://doi.org/10.1016/j.actamat.2015.07.049.

[24] D. Raabe, M. Herbig, S. Sandlöbes, Y. Li, D. Tytko, M. Kuzmina, D. Ponge, P. Choi, Grain boundary segregation engineering in metallic alloys : a pathway to the design of interfaces, Curr. Opin. Solid State Mater. Sci. 18 (2014) 253–261.

[25] M.A. Gibson, C.A. Schuh, Segregation-induced changes in grain boundary cohesion and embrittlement in binary alloys, Acta Mater 95 (2015) 145–155, https://doi.org/10.1016/j.actamat.2015.05.004.
[26] J.R. Trelewicz, C.A. Schuh, Grain boundary segregation and thermodynamically stable binary nanocrystalline alloys, Phys. Rev. B Condens. Matter Mater. Phys. 79 (2009) 1–13, https://doi.org/10.1103/PhysRevB.79.094112.
[27] T.J. Rupert, J.R. Trelewicz, C.A. Schuh, Grain boundary relaxation strengthening of nanocrystalline Ni-W alloys, J. Mater. Res. 27 (2012) 1285–1294, https://doi.org/10.1557/jmr.2012.55.
[28] A. Khalajhedayati, Z. Pan, T.J. Rupert, Manipulating the interfacial structure of nanomaterials to achieve a unique combination of strength and ductility, Nat. Commun. 7 (2016), https://doi.org/10.1038/ncomms10802.
[29] H. Lee, V. Tomar, An examination of nickel doping effect on the mechanical strength of a tungsten grain boundary, Comput. Mater. Sci. 77 (2013) 131–138, https://doi.org/10.1016/j.commatsci.2013.04.034.
[30] P. Lejcek, M. Šob, V. Paidar, Interfacial segregation and grain boundary embrittlement : an overview and critical assessment of experimental data and calculated results, Prog. Mater. Sci. 87 (2017) 83–139, https://doi.org/10.1016/j.pmatsci.2016.11.001.
[31] P. Lejcek, Grain Boundary Segregation in Metals, Springer, Berlin-Heidelberg, 2010, https://doi.org/10.1016/0168-583X(93)95111-H.
[32] C.A. Schuh, M. Kumar, W.E. King, Analysis of grain boundary networks and their evolution during grain boundary engineering, Acta Mater. 51 (2003) 687–700, https://doi.org/10.1016/S1359-6454(02)00447-0.
[33] D. Scheiber, R. Pippan, P. Puschnig, L. Romaner, Ab initio search for cohesion-enhancing impurity elements at grain boundaries in molybdenum and tungsten, Model. Simul. Mater. Sci. Eng. 24 (2016) 85009, https://doi.org/10.1088/0965-0393/24/8/085009.
[34] D. Scheiber, R. Pippan, P. Puschnig, A. Ruban, L. Romaner, Ab-initio search for cohesion-enhancing solute elements at grain boundaries in molybdenum and tungsten, Int. J. Refract. Met. Hard Mater. 60 (2016) 75–81, https://doi.org/10.1016/j.ijrmhm.2016.07.003.
[35] M. Wurmshuber, S. Jakob, S. Doppermann, S. Wurster, R. Bodlos, L. Romaner, V. Maier-Kiener, D. Kiener, Tuning mechanical properties of ultrafine-grained tungsten by manipulating grain boundary chemistry, Acta Mater. 232 (2022), 117939, https://doi.org/10.1016/j.actamat.2022.117939.
[36] S. Wurster, C. Motz, R. Pippan, Notched-cantilever testing on the micrometer scale-effects of constraints on plasticity and fracture behaviour, in: Proceedings of the European Conference on Fracture, 2010.
[37] S. Wurster, C. Motz, R. Pippan, Characterization of the fracture toughness of micro-sized tungsten single crystal notched specimens, Philos. Mag. 92 (2012) 1803–1825, https://doi.org/10.1080/14786435.2012.658449.
[38] J. Ast, M. Ghidelli, K. Durst, M. Göken, M. Sebastiani, A.M. Korsunsky, A review of experimental approaches to fracture toughness evaluation at the micro-scale, Mater. Des. 173 (2019), 107762, https://doi.org/10.1016/j.matdes.2019.107762.
[39] G. Dehm, B.N. Jaya, R. Raghavan, C. Kirchlechner, Overview on micro- and nanomechanical testing: new insights in interface plasticity and fracture at small length scales, Acta Mater. 142 (2018) 248–282, https://doi.org/10.1016/j.actamat.2017.06.019.
[40] A.K. Saxena, S. Brinckmann, B. Völker, G. Dehm, C. Kirchlechner, Experimental conditions affecting the measured fracture toughness at the microscale: notch geometry and crack extension measurement, Mater. Des. 191 (2020), 108582, https://doi.org/10.1016/j.matdes.2020.108582.
[41] B.N. Jaya, C. Kirchlechner, G. Dehm, Can microscale fracture tests provide reliable fracture toughness values? A case study in silicon, J. Mater. Res. 30 (2015) 686–698, https://doi.org/10.1557/jmr.2015.2.
[42] M. Alfreider, S. Kolitsch, S. Wurster, D. Kiener, An analytical solution for the correct determination of crack lengths via cantilever stiffness, Mater. Des. 194 (2020), 108914, https://doi.org/10.1016/j.matdes.2020.108914.
[43] J. Ast, J.J. Schwiedrzik, J. Wehrs, D. Frey, M.N. Polyakov, J. Michler, X. Maeder, The brittle-ductile transition of tungsten single crystals at the micro-scale, Mater. Des. 152 (2018) 168–180, https://doi.org/10.1016/j.matdes.2018.04.009.
[44] D.E.J. Armstrong, C.D. Hardie, J. Gibson, A.J. Bushby, P.D. Edmondson, S. G. Roberts, Small-scale characterisation of irradiated nuclear materials: part II nanoindentation and micro-cantilever testing of ion irradiated nuclear materials, J. Nucl. Mater. 462 (2015) 374–381, https://doi.org/10.1016/j.jnucmat.2015.01.053.
[45] F. Iqbal, J. Ast, M. Göken, K. Durst, *In situ* micro-cantilever tests to study fracture properties of NiAl single crystals, Acta Mater. 60 (2012) 1193–1200, https://doi.org/10.1016/j.actamat.2011.10.060.
[46] R. Pippan, S. Wurster, D. Kiener, Fracture mechanics of micro samples: fundamental considerations, Mater. Des. 159 (2018) 252–267, https://doi.org/10.1016/J.MATDES.2018.09.004.
[47] P. Hosemann, C. Shin, D. Kiener, Small scale mechanical testing of irradiated materials, J. Mater. Res. 30 (2015) 1231–1245, https://doi.org/10.1557/jmr.2015.26.
[48] D. Kiener, A.M. Minor, O. Anderoglu, Y. Wang, S.A. Maloy, P. Hosemann, Application of small-scale testing for investigation of ion-beam-irradiated materials, J. Mater. Res. 27 (2012) 2724–2736, https://doi.org/10.1557/jmr.2012.303.
[49] P. Hosemann, Small-scale mechanical testing on nuclear materials: bridging the experimental length-scale gap, Scr. Mater. 143 (2018) 161–168, https://doi.org/10.1016/j.scriptamat.2017.04.026.
[50] A. Xu, C. Beck, D.E.J. Armstrong, K. Rajan, G.D.W. Smith, P.A.J. Bagot, S. G. Roberts, Ion-irradiation-induced clustering in W – *Re* and W – *Re* – Os alloys : a comparative study using atom probe tomography and nanoindentation measurements, Acta Mater. 87 (2015) 121–127, https://doi.org/10.1016/j.actamat.2014.12.049.
[51] R. Henry, I. Zacharie-Aubrun, T. Blay, N. Tarisien, S. Chalal, X. Iltis, J.M. Gatt, C. Langlois, S. Meille, Irradiation effects on the fracture properties of UO2 fuels studied by micro-mechanical testing, J. Nucl. Mater. (2020) 536, https://doi.org/10.1016/j.jnucmat.2020.152179.
[52] C. Gasparrini, A. Xu, K. Short, T. Wei, J. Davis, T. Palmer, D. Bhattacharyya, L. Edwards, M.R. Wenman, Micromechanical testing of unirradiated and helium ion irradiated SA508 reactor pressure vessel steels: nanoindentation vs *in-situ* microtensile testing, Mater. Sci. Eng. A (2020) 796, https://doi.org/10.1016/j.msea.2020.139942.
[53] J.S. Weaver, S. Pathak, A. Reichardt, H.T. Vo, S.A. Maloy, P. Hosemann, N.A. Mara, Spherical nanoindentation of proton irradiated 304 stainless steel: a comparison of small scale mechanical test techniques for measuring irradiation hardening, J. Nucl. Mater. 493 (2017) 368–379, https://doi.org/10.1016/j.jnucmat.2017.06.031.
[54] F.M. Halliday, D.E.J. Armstrong, J.D. Murphy, S.G. Roberts, Nanoindentation and micromechanical testing of iron-chromium alloys implanted with iron ions, Adv. Mater. Res. 59 (2008) 304–307, https://doi.org/10.4028/www.scientific.net/amr.59.304.
[55] D.E.J. Armstrong, X. Yi, E.A. Marquis, S.G. Roberts, Hardening of selfion implanted tungsten and tungsten 5-wt% rhenium, J. Nucl. Mater. 432 (2013) 428–436, https://doi.org/10.1016/j.jnucmat.2012.07.044.
[56] D.E.J. Armstrong, P.D. Edmondson, S.G. Roberts, Effects of sequential tungsten and helium ion implantation on nano-indentation hardness of tungsten, Appl. Phys. Lett. 102 (2013), 251901.
[57] M. Wurmshuber, S. Doppermann, S. Wurster, D. Kiener, Ultrafine-grained tungsten by high-pressure torsion – bulk precursor versus powder processing route, IOP Conf. Ser. Mater. Sci. Eng. 580 (2019), 012051, https://doi.org/10.1088/1757-899X/580/1/012051.
[58] M.J. Pfeifenberger, M. Mangang, S. Wurster, J. Reiser, A. Hohenwarter, W. Pfleging, D. Kiener, R. Pippan, The use of femtosecond laser ablation as a novel tool for rapid micro-mechanical sample preparation, Mater. Des. 121 (2017) 109–118, https://doi.org/10.1016/j.matdes.2017.02.012.
[59] ASTM Standard E 399-09, ASTM International, 2009.
[60] D. Rajpoot, P. Tandaiya, R.L. Narayan, U. Ramamurty, Size effects and failure regimes in notched micro-cantilever beam fracture, Acta Mater. 234 (2022), 118041, https://doi.org/10.1016/j.actamat.2022.118041.
[61] ASTM Standard E 813-89, ASTM International, 1989.
[62] M. Alfreider, D. Kozic, O. Kolednik, D. Kiener, In-situ elastic-plastic fracture mechanics on the microscale by means of continuous dynamical testing, Mater. Des. 148 (2018) 177–187, https://doi.org/10.1016/j.matdes.2018.03.051.
[63] M. Burtscher, M. Alfreider, K. Schmuck, H. Clemens, S. Mayer, D. Kiener, *In situ* fracture observations of distinct interface types within a fully lamellar intermetallic TiAl alloy, J. Mater. Res. (2020), https://doi.org/10.1557/jmr.2020.306.
[64] J. Ast, B. Merle, K. Durst, M. Göken, Fracture toughness evaluation of NiAl single crystals by microcantilevers - a new continuous J-integral method, J. Mater. Res. 31 (2016) 3786–3794, https://doi.org/10.1557/jmr.2016.393.
[65] K. Schmuck, M. Alfreider, D. Kiener, Crack length estimations for small scale fracture experiments via image processing techniques, J. Mater. Res. 37 (2022) 2848–2861, https://doi.org/10.1557/s43578-022-00681-4.
[66] M. Alfreider, J. Zechner, D. Kiener, Addressing fracture properties of individual constituents within a Cu-{WTi}-{SiOx}-Si multilayer, JOM 72 (2020) 4551–4558, https://doi.org/10.1007/s11837-020-04444-6.
[67] M. Alfreider, R. Bodlos, L. Romaner, D. Kiener, The influence of chemistry on the interface toughness in a {WTi}-Cu system, Acta Mater. (2022), 117813, https://doi.org/10.1016/j.actamat.2022.117813.
[68] J. Ast, M. Göken, K. Durst, Size-dependent fracture toughness of tungsten, Acta Mater. 138 (2017) 198–211, https://doi.org/10.1016/j.actamat.2017.07.030.
[69] I. Issa, A. Hohenwarter, R. Fritz, D. Kiener, Fracture properties of ultrafine grain chromium correlated to single dislocation processes at room temperature, J. Mater. Res. 34 (2019) 2370–2383, https://doi.org/10.1557/jmr.2019.140.
[70] C. Bohnert, N.J. Schmitt, S.M. Weygand, O. Kraft, R. Schwaiger, Fracture toughness characterization of single-crystalline tungsten using notched micro-cantilever specimens, Int. J. Plast. 81 (2016) 1–17, https://doi.org/10.1016/j.ijplas.2016.01.014.
[71] ASTM Standard E 1820-13, ASTM International, 2013.
[72] D. Kiener, R. Fritz, M. Alfreider, A. Leitner, R. Pippan, V. Maier-Kiener, Rate limiting deformation mechanisms of bcc metals in confined volumes, Acta Mater. 166 (2019) 687–701, https://doi.org/10.1016/J.ACTAMAT.2019.01.020.
[73] R. Fritz, V. Maier-Kiener, D. Lutz, D. Kiener, Interplay between sample size and grain size: single crystalline vs. ultrafine-grained chromium micropillars, Mater. Sci. Eng. A 674 (2016) 626–633, https://doi.org/10.1016/j.msea.2016.08.015.
[74] R. Fritz, D. Wimler, A. Leitner, V. Maier-Kiener, D. Kiener, Dominating deformation mechanisms in ultrafine-grained chromium across length scales and temperatures, Acta Mater. 140 (2017) 176–187, https://doi.org/10.1016/j.actamat.2017.08.043.
[75] T.L. Anderson, Fracture Mechanics: Fundamentals and Applications, 4th ed., Taylor & Francis Group, Boca Raton, 2017.
[76] C.F. Shih, Relationship between the J-integral and the COD for stationary and extending cracks, J. Mech. Phys. Solids 29 (1981) 305–326.
[77] O. Kolednik, P. Kutleša, On the influence of specimen geometry on the critical crack-tip-opening displacement, Eng. Fract. Mech. 33 (1989) 215–223, https://doi.org/10.1016/0013-7944(89)90025-8.
[78] T. Pardoen, F. Hachez, B. Marchioni, P.H. Blyth, A.G. Atkins, Mode I fracture of sheet metal, J. Mech. Phys. Solids. 52 (2004) 423–452, https://doi.org/10.1016/S0022-5096(03)00087-5.

[79] T. Pardoen, Y. Marchal, F. Delannay, Thickness dependence of cracking resistance in thin aluminium plates, 1999. doi:10.1016/S0022-5096(99)00011-3.
[80] G. Dhondt, The Finite Element Method for Three-Dimensional Thermomechanical Applications, John Wiley & Sons, Ltd, Chichester, UK, 2004, https://doi.org/10.1002/0470021217.
[81] G.R. Irwin, Fracture Dynamics, Fracturing of Metals, American Society for Metals, Cleveland, 1948.
[82] N.A. Fleck, J.W. Hutchinson, Strain gradient plasticity, Adv. Appl. Mech. 33 (1997) 295–361, https://doi.org/10.1016/S0065-2156(08)70388-0.
[83] T.J. Massart, T. Pardoen, Strain gradient plasticity analysis of the grain-size-dependent strength and ductility of polycrystals with evolving grain boundary confinement, Acta Mater. 58 (2010) 5768–5781, https://doi.org/10.1016/j.actamat.2010.06.052.
[84] R. Russo, F.A.G. Mata, S. Forest, D. Jacquin, A review on strain gradient plasticity approaches in simulation of manufacturing processes, J. Manuf. Mater. Process. 4 (2020) 87, https://doi.org/10.3390/jmmp4030087.
[85] M. Elices, G.V. Guinea, J. Gómez, J. Planas, The cohesive zone model: advantages, limitations and challenges, Eng. Fract. Mech. 69 (2001) 137–163, https://doi.org/10.1016/S0013-7944(01)00083-2.
[86] W. Węglewski, P. Pitchai, K. Bochenek, G. Bolzon, R. Konetschnik, B. Sartory, R. Ebner, D. Kiener, M. Basista, Experimental and numerical investigation of the deformation and fracture mode of microcantilever beams made of Cr(*Re*)/Al_2O_3 metal–matrix composite, Metall. Mater. Trans. A Phys. Metall. Mater. Sci. 51 (2020) 2377–2390, https://doi.org/10.1007/s11661-020-05687-3.
[87] B. Gludovatz, S. Wurster, A. Hoffmann, R. Pippan, Fracture toughness of polycrystalline tungsten alloys, Int. J. Refract. Met. Hard Mater. 28 (2010) 674–678, https://doi.org/10.1016/j.ijrmhm.2010.04.007.